



Spin Crossover

Thermal and Light-Induced Spin Transitions of Fe^{II} Complexes with 4- and 5-(Phenylazo)-2,2'-bipyridine Ligands: Intra- vs. Intermolecular EffectsSven Olaf Schmidt,^[a] Holger Naggert,^[a] Axel Buchholz,^[b] Hannah Brandenburg,^[a] Alexander Bannwarth,^[a] Winfried Plass,^[b] and Felix Tuczek*^[a]

Dedicated to Professor Dr. Philipp Gütllich on the occasion of his 80th birthday

Abstract: Five new spin crossover complexes with 4- and 5-(phenylazo)-2,2'-bipyridine (4-/5-PABipy) ligands were synthesized and investigated with respect to their spin crossover (SCO) behavior. The results are compared to the thermal and light-induced spin transition properties of the parent SCO complexes [Fe(bpz)₂(bipy)] (**1**) and [Fe(bipy)₂(NCS)₂] (**2**). [Fe(bpz)₂(4-PABipy)] (**1a**) undergoes a stepwise spin transition whereas [Fe(bpz)₂(5-PABipy)] (**1b**) exhibits a one-step transition with a 6 K-wide hysteresis. For [Fe(bpz)₂(^tBu5-PABipy)] (**1c**) the spin

transition to the low-spin state is incomplete. Qualitatively similar changes of the SCO behavior are observed for the complexes [Fe(4-PABipy)₂(NCS)₂] (**2a**) and [Fe(5-PABipy)₂(NCS)₂] (**2b**). In comparison to the parent system **2**, a strengthening of intermolecular interactions leads to a stabilization of the low-spin state. Evidence for the LIESST behavior could be obtained for all new compounds by means of magnetic susceptibility measurements as well as UV/Vis and resonance Raman spectroscopy.

Introduction

Eight decades after the discovery of the spin crossover (SCO) phenomenon^[1] the exploration of new SCO complexes is still an active and fascinating field of research. Most of these systems are based on iron(II),^[2] which can exist in a diamagnetic low-spin ($S = 0$) and a paramagnetic high-spin ($S = 2$) state. The possibility to switch between these two states makes SCO complexes interesting as building blocks for molecular electronics, spintronics^[3–8] or memory devices.^[9] For these purposes light might be the most effective stimulus, and in fact different mechanisms of light-induced spin change have been established over the past decades.^[10–15] With regard to possible applications, the spin change has to occur rapidly, reversibly, and preferably at room temperature. Due to the relatively low barrier between the ⁵T₂ excited and the ¹A₁ ground state, the LIESST effect (light-induced excited spin state trapping) is usually observed at low temperatures.^[10,16,17] The LD-LISC (ligand-driven light-induced spin change) and LD-CISSS (light-driven coordination-induced spin state switching) effects, on the other

hand, have been employed to realize photoinduced spin-state switching at room temperature and in solution.^[13,18,19]

Possible photoactive substituents which might be employed in LD-LISC systems to switch the ligand-field strength of coordinated ligands are phenylazo groups. Earlier we analyzed iron(III) salen complexes [salten = azaheptamethylene-1,7-bis(salicylideneimine)]^[20–24] with one photoswitchable phenylazopyridine (PAP) ligand.^[25] However, the PAP ligands were found to be labile towards photodissociation. So we decided to synthesize more photostable 2,2'-bipyridine ligands with phenylazo substituents (= PABipy ligands) and explore the LD-LISC properties of derived Fe^{II} complexes. Specifically, we attached phenylazo moieties in 4- and 5-position to the 2,2'-bipyridine unit, leading to the ligands 4-(phenylazo)-2,2'-bipyridine (4-PABipy) and 5-(phenylazo)-2,2'-bipyridine (5-PABipy). The impact of an additional bulky substituent in these systems was explored by introduction of a *tert*-butyl substituent in the 5-PABipy ligand, generating the ^tBu5-PABipy ligand.

In order to determine how the new PABipy ligands influence the electronic and magnetic properties of Fe^{II} SCO complexes, we used them in place of the unsubstituted bipy counterparts as ligands for the classic SCO systems [Fe(bpz)₂(bipy)] {bpz = dihydrobis(pyrazolyl)borate}^[14,19,26–32] (**1**) and [Fe(bipy)₂(NCS)₂] (**2**).^[33–35] The resulting new complexes [Fe(bpz)₂(4-PABipy)] (**1a**), [Fe(bpz)₂(5-PABipy)] (**1b**), [Fe(bpz)₂(^tBu5-PABipy)] (**1c**) as well as [Fe(4-PABipy)₂(NCS)₂] (**2a**) and [Fe(5-PABipy)₂(NCS)₂] (**2b**) were intensively studied in solution as potential LD-LISC systems.^[36] In the course of these investigations, however, it became apparent that these systems also exhibit unusual solid-state SCO

[a] Institut für Anorganische Chemie, Christian-Albrechts-Universität Kiel, Max-Eyth-Str. 2, 24118 Kiel, Germany
E-mail: ftuczek@ac.uni-kiel.de
<https://www.ac.uni-kiel.de/de/tuczek>

[b] Institut für Anorganische und Analytische Chemie, Friedrich-Schiller-Universität Jena, Humboldtstr. 8, 07743 Jena, Germany

Supporting information for this article is available on the WWW under <http://dx.doi.org/10.1002/ejic.201501252>.

properties which are of interest in their own right. Herein these results are presented, analyzed and compared to corresponding data obtained with the parent complexes $[\text{Fe}(\text{bpz})_2(\text{bipy})]$ (**1**) and $[\text{Fe}(\text{bipy})_2(\text{NCS})_2]$ (**2**), respectively.

The influence of a functionalization of 2,2'-bipyridine on the SCO properties of SCO complexes with bipy coligands has been studied before. Complex **1** exhibits a $T_{1/2}$ of 160 K^[26] whereas the spin transition temperature of complex **2** has been determined to 213 K.^[33–35] Introduction of a styryl group in 4-position and a methyl-group in 4'-position was found to lead to $T_{1/2}$ values of 264 K and 380 K for the complex $[\text{Fe}(\text{t-mstbpy})_2(\text{NCS})_2]$, respectively.^[37] Besides changing the SCO temperature, functionalization of bipy with large side groups will also modify long and short-range intermolecular interactions between the complex molecules which strongly influence the SCO process.^[38–41] These effects were also studied for a series of $[\text{Fe}(\text{bpz})_2(\text{L})]$ ^[31,42] and $[\text{Fe}(\text{L})_2(\text{NCS})_2]$ ^[41,43–45] complexes and will be analyzed for our new complexes as well.

Results and Discussion

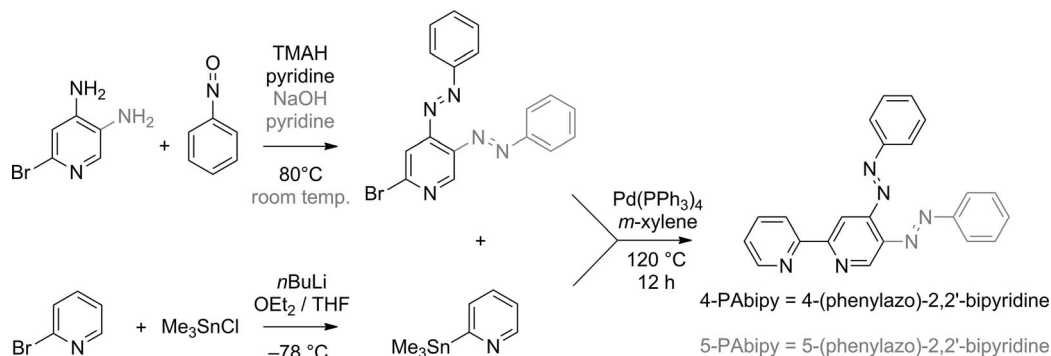
Syntheses

The ligands have been prepared by a 3-step synthesis involving literature-known procedures,^[46–49] starting from 4/5-amino-2-

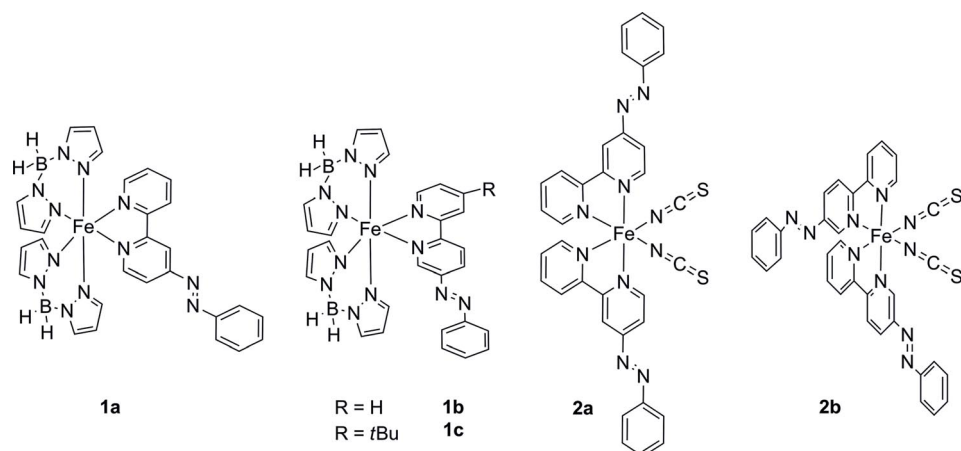
bromopyridine which reacts with nitrosobenzene in a Mills-reaction to 2-bromo-(4/5)-(phenylazo)pyridine. In the next step this compound is used in a Stille-coupling with 2-trimethylstannylpyridine, which was prepared by reaction of 2-bromopyridine and trimethyltin chloride. This synthetic route is different to the literature-known procedure for the preparation of 4/5-(phenylazo)-2',2'-bipyridines (Scheme 1).^[50–52] *tert*-Butyl functionalized 5-(phenylazo)bipyridine is prepared in a slightly different way: 4-(*tert*-butyl)pyridine is stannylated by tri-*n*-butyltin chloride in hexane; afterwards Stille coupling with the 2-bromo-5-(phenylazo)pyridine leads to the target ^tBu-5-PAbipy ligand.

Based on the phenylazo-functionalized bipyridine ligands, four new spin crossover complexes were synthesized: $[\text{Fe}(\text{bpz})_2(4\text{-PAbipy})]$ (**1a**), $[\text{Fe}(\text{bpz})_2(5\text{-PAbipy})]$ (**1b**), $[\text{Fe}(\text{bpz})_2(\text{t}^{\text{Bu}}5\text{-PAbipy})]$ (**1c**), $[\text{Fe}(4\text{-PAbipy})_2(\text{NCS})_2]$ (**2a**) and $[\text{Fe}(5\text{-PAbipy})_2(\text{NCS})_2]$ (**2b**) (Scheme 2). The synthesis of complexes **1a** and **1b** started from $\text{Fe}(\text{ClO}_4)_2$ hexahydrate in methanolic solution. First, a solution of potassium dihydro(bispyrazolyl)borate was added and precipitated KClO_4 was removed by filtration.^[26] After addition of phenylazobipyridine, dissolved in methanol, a dark blue-greenish powder in the case of complex **1a** and light green solids for complexes **1b** and **1c** were obtained.

For the synthesis of complexes **2a** and **2b** iron(II) trifluoromethanesulfonate was used as precursor and the synthesis was



Scheme 1. Ligand syntheses of 4-(phenylazo)-2,2'-bipyridine (4-PAbipy) and 5-(phenylazo)-2,2'-bipyridine (5-PAbipy).



Scheme 2. New iron spin-crossover complexes with phenylazo-functionalized 2,2'-bipyridine ligands (PAbipy): $[\text{Fe}(\text{bpz})_2(4\text{-PAbipy})]$ (**1a**), $[\text{Fe}(\text{bpz})_2(5\text{-PAbipy})]$ (**1b**), $[\text{Fe}(\text{bpz})_2(5\text{-t}^{\text{Bu}}\text{PAbipy})]$ (**1c**), $[\text{Fe}(4\text{-PAbipy})_2(\text{NCS})_2]$ (**2a**), $[\text{Fe}(5\text{-PAbipy})_2(\text{NCS})_2]$ (**2b**).

performed in acetonitrile. Solid potassium thiocyanate was added and a solution of the phenylazobipyridine in CH_3CN was added to this suspension. After heating to 80 °C for 1 h the desired complexes precipitated and were isolated by filtration, yielding a blue solid in the case of compound **2a** and a green solid for complex **2b**. Efforts to isolate $[\text{Fe}(\text{t}^{\text{Bu}}\text{5-PAbipy})_2(\text{NCS})_2]$ (**2c**) prepared in an analogous fashion failed.

1. $[\text{Fe}(\text{bpz})_2(\text{L})]$, L = 4-PAbipy, 5-PAbipy and $\text{t}^{\text{Bu}}\text{5-PAbipy}$

a) Thermal and Light-Induced Spin Crossover

The SCO properties of the new complexes $[\text{Fe}(\text{bpz})_2(\text{L})]$, L = 4-PAbipy (**1a**), 5-PAbipy (**1b**) and $\text{t}^{\text{Bu}}\text{5-PAbipy}$ (**1c**) were first investigated with a PPMS and a SQUID magnetometer equipped with an irradiation unit, respectively. In case of **1a** the transition from low-spin to high-spin occurs in a very gradual fashion in a temperature interval ranging from ca. 20 to 190 K. Between 100 and 150 K a steeper SCO transition is observed, and between 190 and 195 K a second, abrupt transition occurs (Figure 1). Both, the steeper and the abrupt change of μ_{eff} occur in a temperature interval of ± 70 K around the $T_{1/2}$ value of the parent system **1** (grey points in Figure 1). Irradiation of **1a** at 20 K with $\lambda_{\text{exc}} = 510$ nm causes a spin transition of about 20 % (red). The population of the metastable $^5\text{T}_2$ state persists up to ca. 50 K where it relaxes to the $^1\text{A}_1$ ground state. At ca. 70 K the warm-up curve of the irradiated sample (red) and the cooling curve (blue) of **1a** are identical.

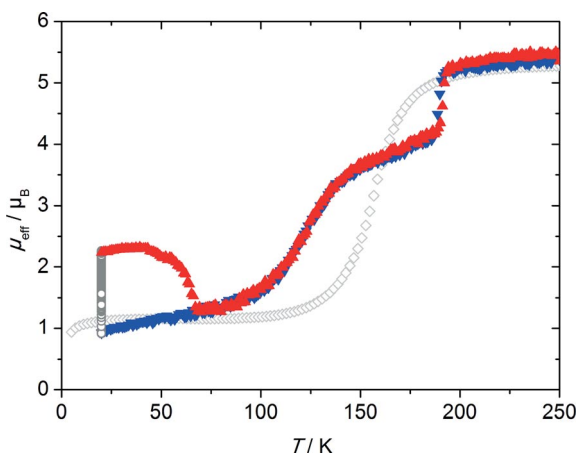


Figure 1. μ_{eff} vs. T for $[\text{Fe}(\text{bpz})_2(4\text{-PAbipy})]$ (**1a**). Blue: cooling, grey circles: irradiation at 20 K with 510 nm, red: heating after irradiation. Grey diamonds: μ_{eff} vs. T plot of $[\text{Fe}(\text{bpz})_2(\text{bipy})]$ (**1**).

In case of **1b** the spin transition of **1** does not change to a stepwise characteristics as observed for **1a**, but instead globally shifts to lower temperature (95 K; Figure 2). It is steeper than in **1** and exhibits a 6 K-wide hysteresis. These features indicate an increase of cooperative intermolecular interactions with respect to the parent system **1**.^[2] Irradiation of **1b** under the same conditions as applied for **1a** leads to a ca. 30 % population of the metastable high-spin state which persists up to 60 K (red).

In order to weaken the intermolecular interactions which cause the hysteresis observed for **1b** (see below), a *tert*-butyl group was introduced in the 5-PAbipy ligand in 4'-position,

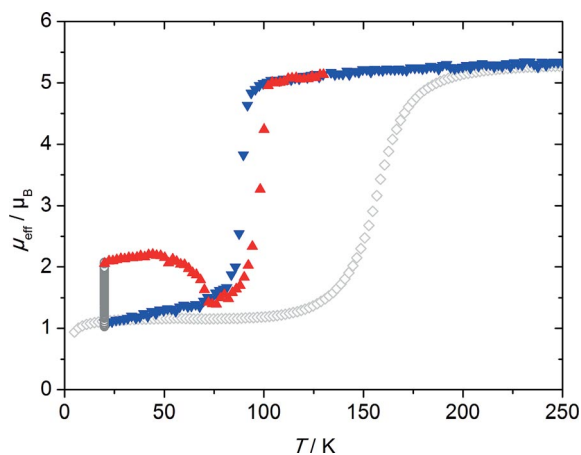


Figure 2. μ_{eff} vs. T for $[\text{Fe}(\text{bpz})_2(5\text{-PAbipy})]$ (**1b**). Blue: cooling, grey circles: irradiation at 20 K with 510 nm, red: heating after irradiation. Grey diamonds: μ_{eff} vs. T plot of $[\text{Fe}(\text{bpz})_2(\text{bipy})]$ (**1**).

leading to complex **1c**. Unexpectedly, this substitution was found to largely suppress the thermal spin transition (Figure 3). Upon warming up a sample of **1c** which before was slowly cooled down to 5 K (blue curve in Figure 3) the magnetic moment first increases from ≈ 3 to $\approx 3.5 \mu_{\text{B}}$ (magenta curve in Figure 3). In the temperature range between 20 and 80 K there is only a slight increase of the magnetic moment detectable. At

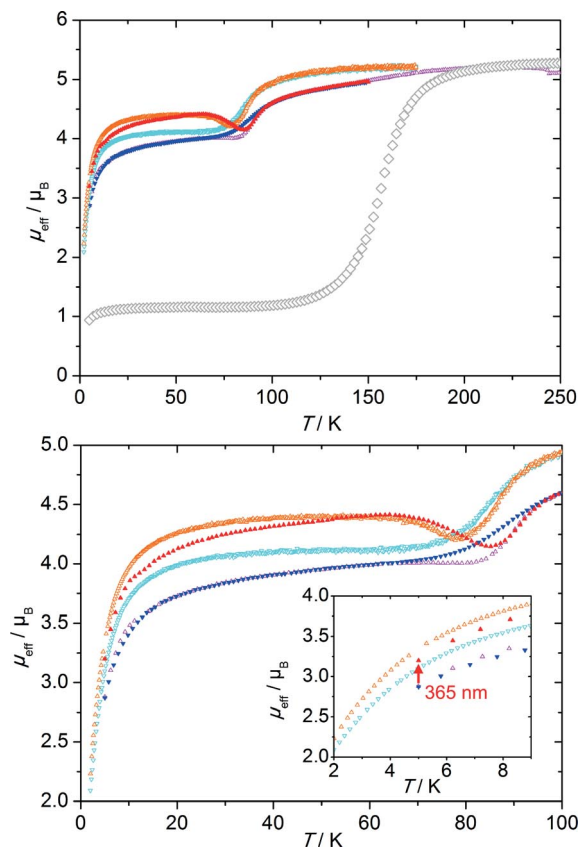


Figure 3. μ_{eff} vs. T for $[\text{Fe}(\text{bpz})_2(5\text{-t}^{\text{Bu}}\text{PAbipy})]$ (**1c**), \diamond : $[\text{Fe}(\text{bpz})_2(\text{bipy})]$, red: warming; blue: cooling; magenta: warming without irradiation, cyan: cooling of TIESST experiment, orange: warming after rapid cooling. Bottom: detailed region < 100 K. Inset: detailed view on the photoexcitation of **1c** < 10 K.

85 K a small, gradual spin transition occurs, and between 100 and 250 K again a very gradual increase of μ_{eff} is observed. Around 80 K, the cooling curve (blue) exhibits a slightly more gradual spin transition than the heating curve (magenta; Figure 3).

Irradiation of the slowly cooled-down sample at 5 K with $\lambda_{\text{exc}} = 365$ nm increases μ_{eff} from 2.87 to 3.20 μ_{B} , corresponding to a partial population of the metastable high-spin state (Figure 3, bottom, red arrow). Warming up the irradiated sample leads to a similar increase of μ_{eff} as observed for the unirradiated sample, but shifted to higher values by an offset of ca. 0.5 μ_{B} (red curve in Figure 3). The population of the metastable high-spin state persists up to ca. 60 K where the system relaxes to the thermal state of the unirradiated sample.

It is also possible to trap the excited spin state in complex **1c** by rapid cooling of the sample down to 2 K. Subsequent warming to room temperature (orange curve in Figure 3) leads to nearly the same characteristics as found for warming the sample which was irradiated at low temperature (red curve). Obviously a fraction of SCO molecules has been frozen in the high-spin state due to the rapid cooling process (TIESST, temperature-induced excited spin-state-trapping).^[53–58] Around 80 K there is a dip in the μ_{eff} vs. T curve which is caused by relaxation of the metastable high-spin state, and at 82 K a thermal spin transition occurs which leads to saturation of μ_{eff} at ca. 120 K. Slow recooling of the sample from room temperature to 5 K exhibits a characteristics which above 100 K is congruent with the warming curve, but at temperatures < 80 K does not show the TIESST effect (Figure 3, cyan curve). Nevertheless, the magnetic moments are globally higher in this curve than in the sample which has not been subjected to initial rapid cooling.

Incomplete or even fully suppressed SCO transitions have been observed for other $[\text{Fe}(\text{bpz})_2(\text{L})]$ complexes.^[31,42] These findings have been explained by π - π stacking interactions.^[31,42] This way, the bidentate coligands L become interdigitated, which also strongly influences the crystal packing. In such an arrangement, the *tert*-butyl group in the PABipy backbone further hinders the contraction of all complex molecules during transformation to the low-spin state by blocking intermolecular motions.

In summary, major, characteristic changes have been detected between the thermal SCO properties of the new complexes **1a–1c** and the parent system $[\text{Fe}(\text{bpz})_2(\text{bipy})]$ (**1**).^[26] The most simple effect is observed for **1b** containing the 5-phenylazo ligand where the entire spin transition curve is shifted by about 65 K to lower temperature with respect to **1**. This indicates a weakening of the ligand-field strength of 5-PABipy compared to unsubstituted 2,2'-bipyridine. The phenylazo unit is an electron-withdrawing group, which decreases the electron density in the bipyridine backbone and thus leads to a decrease of the σ -donor strength. The phenylazo unit is located at 5-position, so the conjugated π -system is not enlarged to enhance the π -acceptor properties, but the attachment of the phenylazo unit in 5-position increases the π - π stacking capabilities compared to complex **1**. Assuming the common stacking motif for this type of complexes^[31,42] the phenylazo group in complex **1b** is located orthogonally to the Fe–Fe axis. This leads

to the same intermolecular iron–iron distance but to a stronger “interdimer coupling” compared to the parent system **1**, caused by π - π stacking. We assume that this increase of cooperativity leads to the observed 6 K-wide hysteresis.

In case of complex **1a** the one-step spin transition of **1** is modified to a stepwise characteristics, centered around the $T_{1/2}$ value of the parent complex **1**.^[26] So, the ligand-field strength does not appear to change greatly whereas the characteristics of the spin transition is influenced by additional intermolecular interactions. The phenylazo substituent in 4-position enhances the π -acceptor capability of the bipy ligand, which should act to increase the ligand field strength. On the other hand, the electron-withdrawing effect of the PA group lowers the σ -donor strength (see above); obviously, in the case of the 4-PABipy ligand both effects cancel each other.

Usually, a two-step spin transition results from an “antiferromagnetic” coupling between the low-spin and the high-spin species.^[2] With regard to **1a**, π - π interactions between two bipyridine units and/or two 4-phenylazo substituents of neighbouring complex molecules could lead to a situation where an alternating high-spin/low-spin arrangement of SCO complexes is favoured. The low-temperature part of the two-step transition appears to be associated with such a case. The gradual characteristics could be due to short-range, intermolecular interactions that are comparatively “soft”. The much steeper high-temperature part of the two-step transition, on the other hand, can be attributed to a transition to the high-spin state that is associated with long-range, cooperative interactions. The thermal spin transition in **1c**, finally, is largely suppressed as this system is “locked” in the high-spin state due to intermolecular interactions that hinder the relative motion of the complexes in the crystal lattice.

The LIESST properties of **1a**, **1b** and **1c** are also influenced by the different ligand field strengths of the bipy ligands. According to the “inverse energy-gap” law,^[16,17] the tunneling rate constant k_{HL} of the high-spin \rightarrow low-spin relaxation increases with an increasing energy gap ΔE_{HL} between the $^1\text{A}_1$ and the $^5\text{T}_2$ state which in turn is related to $T_{1/2}$.^[16] This explains why the light-induced metastable high-spin states in **1b** and **1c** are stable over a larger temperature range compared to complex **1a**: The minima of the $(\partial\mu_{\text{eff}}/\partial T)$ curves (corresponding to T_{LIESST})^[59] are located at 67 K for **1a**, 70 K for **1b** and 80 K for **1c**; see Supporting Information, Figures S1–S3) whereas T_{LIESST} of **1** under the same experimental conditions is determined to 52 K.^[36]

b) ^{57}Fe -Mössbauer Spectroscopy

In order to obtain further information on the spin transitions of **1a–1c** temperature-dependent Mössbauer spectroscopy was employed. In complex **1a** (Figure 4) one doublet with an isomer shift δ_{IS} of 0.46 mm/s and a small quadrupole splitting ΔE_{Q} of 0.68 mm/s is observed at 80 K; these parameters are characteristic for an iron(II) species in the low-spin state.^[60] At about 100 K a new doublet with a large quadrupole splitting emerges, which can be assigned to the high-spin-state. Starting from this temperature, the high-spin doublet further increases and the low-spin doublet further decreases in intensity. As observed in the susceptibility measurements the “high-temperature” SCO of

the two-step curve occurs abruptly at ca. 190 K (Figure 1). This is confirmed by the Mössbauer spectra at 190 and 200 K: whereas the 190 K spectrum clearly shows the contribution of the low-spin species, the 200 K mainly consists of the high-spin species. In the latter spectrum, however, there is a small intensity present between the two components of the high-spin doublet which cannot be fitted by a simple (low-spin) doublet. The residual intensity rather exhibits an asymmetric line shape with a quadrupole splitting between that of the high-spin and the low-spin species. This spectrum may be associated with a fast high-spin/low spin relaxation process,^[61–65] which was also observed in the homoleptic complex [Fe(HB(pz)₃)₂] at high temperatures.^[65] The 300 K Mössbauer spectrum contains a small contribution of the fast relaxing species as well. The fact that the relative intensity of this species is even larger than at 200 K is ascribed to differences in the temperature dependence of the Debye–Waller-factor.^[60]

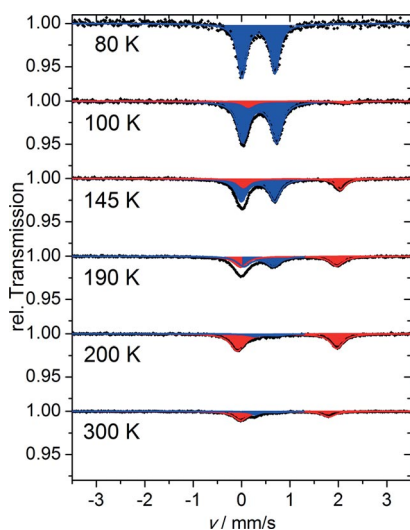


Figure 4. Mössbauer spectra of complex **1a**. Blue: low-spin, red: high-spin.

The Mössbauer spectra of complex **1b** show the thermal behavior expected for a generic SCO compound (Figure 5).

At 80 K one doublet with an isomer shift of 0.53 mm/s and a small quadrupole splitting of 0.63 mm/s characteristic for an iron(II) species in the low-spin state is observed.^[60] Heating the sample to 90 K leads to the appearance of a high-spin signal with an isomer shift of 1.15 mm/s and a quadrupole splitting of 2.74 mm/s. Upon further heating by five degrees the spin transition is almost completed; i.e., the intensity of the high-spin is much higher than that of the low-spin doublet. The spectrum at 300 K exclusively contains the high-spin signal with an isomer shift of 1.01 mm/s and a quadrupole splitting of 2.02 mm/s.

Similar to **1b**, the Mössbauer spectrum of **1c** contains only one doublet at 300 K with parameters characteristic of the high-spin state (Figure 6). Cooling down to 150 K, the doublet of the low-spin state appears which upon further lowering of the temperature increases in intensity. At 80 K the low-spin doublet exhibits an isomer shift δ_{IS} of 0.49 mm/s and a quadrupole splitting ΔE_Q of 0.64 mm/s and the high-spin doublet an isomer shift of 1.11 mm/s and a quadrupole splitting of 2.70 mm/s.

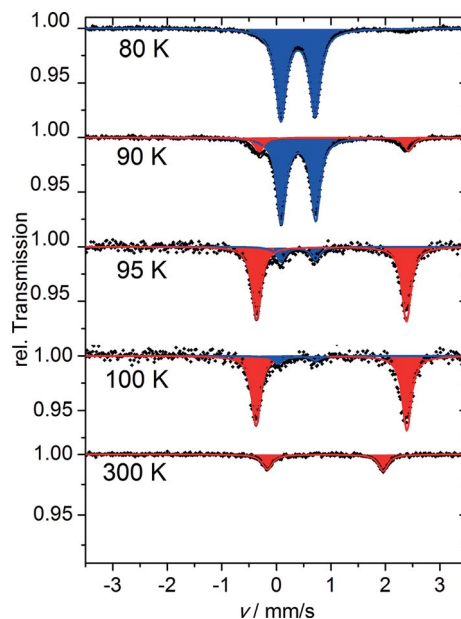


Figure 5. Mössbauer spectra of complex **1b**. Blue: low-spin, red: high-spin.

Between 100 and 80 K, no appreciable change in the relative intensities of high spin and low spin species is observed. These findings correspond to the SQUID data shown in Figure 3 (blue/magenta curves); i.e., between room temperature and 100 K a partial spin transition occurs, which, upon further cooling, leads to a large, temperature-independent high-spin fraction.

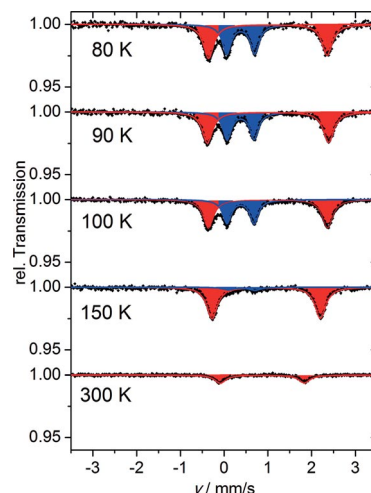


Figure 6. Mössbauer spectra of complex **1c**. Blue: low-spin, red: high-spin.

c) UV/Vis Spectroscopy

In the irradiation experiments conducted in the SQUID magnetometer the light-induced conversion of **1a–1c** to the high-spin state at low temperatures was found to be incomplete (cf Figures 1 and 2, red traces). In order to check whether a larger fraction of the sample can be switched to the metastable high-spin state, LIESST experiments were performed with optically thinner samples in a UV/Vis spectrometer. To this end complexes **1a** and **1b** were pressed with KBr to transparent pellets or deposited as thin films by vacuum evaporation on quartz

discs. Corresponding temperature-dependent spectra are shown in Figure 7. Absorption bands at ca. 290 nm, which appear in the parent complex **1** as well,^[27] result from $\pi\rightarrow\pi^*$ transitions of the aromatic ligands (bipy and bpz). In analogy to Fe^{III} complexes coordinated by phenylazopyridine ligands,^[25] the $\pi\rightarrow\pi^*$ transition of the phenylazo unit is located at 320 nm where it also appears in the spectrum of the vacuum-deposited film of **1a** (Figure 7, top left). The band at 780 nm, which is most intense in the 4 K-spectrum of this complex (blue), results from a Fe \rightarrow 4-PAbipy MLCT transition. Interestingly, this band is shifted to lower energy by about 130 nm compared to the parent complex **1**.^[27] At room temperature the intensity of this band is significantly lowered (red curve). A similar intensity decrease with increasing temperature is also observed for the other bands, with exception of the $\pi\rightarrow\pi^*$ transition of the phenylazo unit. Almost the same intensity decrease (84 %) is observed after irradiation of the sample at 4 K (green curve in Figure 7, top left) with $\lambda_{\text{exc}} = 519$ nm. This indicates a comparable efficiency of spin-state switching as compared to the parent system (85 % intensity reduction). Thermal relaxation of the metastable high-spin-state to the low-spin state the temperature range from 30 to 70 K is indicated by grey spectra. Similar observations are made with **1a** pressed in a KBr disc (Figure 7, bottom left). Here, 780 nm band exhibits vibronic structure with maxima at 707 and 792 nm.

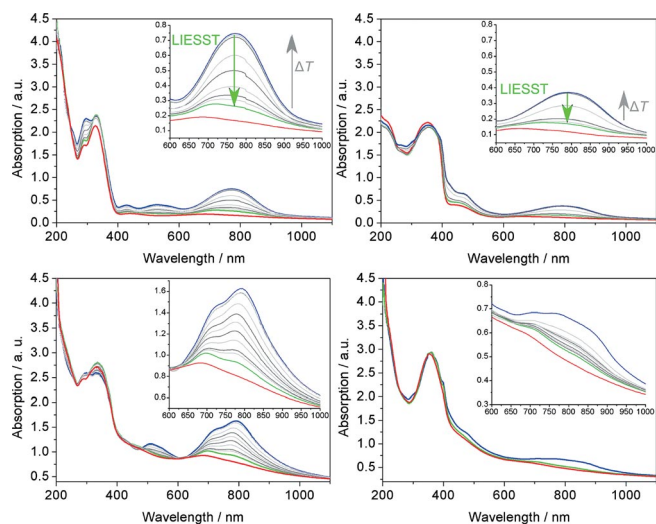


Figure 7. UV/Vis spectra of vacuum deposited films (top) and KBr pellets (bottom) of complex **1a** (left) and **1b** (right). Red: room temperature spectra; green: Irradiation at 4 K for 2 min s; blue: 4 K spectra. Inset: detailed view of the most intensive MLCT absorption band.

The absorption spectra of **1b** show a fairly broad $\pi\rightarrow\pi^*$ transition of the phenylazo unit at 350 nm; at ca. 300 nm the $\pi\rightarrow\pi^*$ transitions of the other aromatic ligands are visible as shoulders (Figure 7, right). With respect to **1a**, the Fe \rightarrow 4-PAbipy MLCT transition is further shifted into the NIR and now is located at ca. 800 nm. Again, it is most intense in the 4 K-spectrum and becomes much weaker at room temperature. Irradiation at 4 K with light of $\lambda_{\text{exc}} = 519$ nm leads to an almost comparable (80 %) intensity reduction. As for **1a**, grey spectra indicate the thermal relaxation of the high spin \rightarrow low spin state which was monitored in temperature range from 30 to 70 K.

In summary, both **1a** and **1b** can be switched to the metastable high-spin state with comparable efficiencies as the parent complex **1**. Moreover, the MLCT transitions of **1a** and **1b** are shifted into the NIR by 130 and 150 nm, respectively, with respect to **1**. These changes are due to the electron-withdrawing effect of the phenylazo groups. For **1a**, the bathochromic shift is less pronounced than for **1b** as it is partly compensated by an increased backbonding capability of the 4-PAbipy ligand with respect to its unsubstituted counterpart (see above).

Finally, the intensity ratio between the Fe \rightarrow PAbipy-MLCT transition and the combined $\pi\rightarrow\pi^*$ -transitions is much larger for the 4- as compared to the 5-PAbipy system. This difference is due to the extension of the π -system in the former ligand, increasing the magnitude of the electric-dipole transition matrix element.^[66] In contrast, the phenylazo group in 5-position only acts to make the bipy ligand less electron-rich. This analysis thus conforms the conclusions drawn from the thermal spin crossover behavior (cf Section a).

2. [Fe(PAbipy)₂(NCS)₂] Complexes

a) Magnetic Susceptibility Measurements

In contrast to the parent spin crossover system [Fe(bipy)₂(NCS)₂] (**2**) where a very steep spin transition occurs at 213 K,^[33–35] the spin transitions of both [Fe(PAbipy)₂(NCS)₂] complexes **2a** and **2b** are more gradual and occur near room temperature (Figure 8). However, there are distinct differences between **2a** and **2b**. The spin transition of **2a** starts at 200 K and is not complete at 400 K (Figure 8, filled triangles). At this temperature the slope of the spin transition curve is small, although with a μ_{eff} of 3.01 B.M. only ca. 55 % of the sample have converted into the high-spin-state yet. In complex **2b** the spin transition proceeds in a similar fashion, but with a μ_{eff} value of 5.12 B.M. is almost completed at 400 K.^[66]

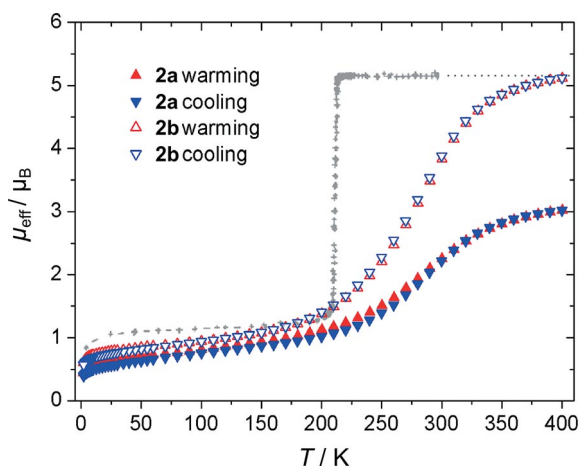


Figure 8. μ_{eff} vs. T for [Fe(4-PAbipy)₂(NCS)₂] (**2a**, filled triangles) and [Fe(5-PAbipy)₂(NCS)₂] (**2b**, empty triangles). Grey: magnetic measurement of [Fe(bipy)₂(NCS)₂], adopted from ref.^[35]

The gradual spin transitions of **2a** and **2b**, as compared to the very steep spin transition of the parent system, can be ascribed to a decrease of cooperative (long-range) interactions

due to the sterically demanding phenylazo groups, which increase the intermolecular distances. Similar conclusions have been drawn by Real et al. who found that for $[\text{Fe}(\text{L})_2(\text{NCS})_2]$ complexes a larger flexibility in the ligand backbone, through, e.g., aliphatic instead of aromatic units, leads to a decrease of cooperativity.^[41] Furthermore, a study on $[\text{Fe}(\text{PM-L})_2(\text{NCS})_2]$ complexes (PM-L = 2'-pyridylmethylene-4-aniline) by Kahn et al. demonstrated that the attachment of a phenylazo unit increases the flexibility of the ligand as compared to other substituents with an aromatic character and thus leads to a decrease of cooperativity.^[67,68]

While the 4- and 5-phenylazo substituents present in both **2a** and **2b** render the spin transition more gradual than in the parent system, they influence the SCO behavior in a different way; i.e., at 400 K the spin transition in **2b** is complete and in **2a** incomplete. If the incomplete spin transition of **2a** is considered as the low-temperature part of a two-step spin transition, introduction of phenylazo substituents into the bipy ligand would have similar effects on the SCO behavior in the $[\text{Fe}(\text{bpz})_2(\text{bipy})]$ and $[\text{Fe}(\text{bipy})_2(\text{NCS})_2]$ systems; i.e., the 5-PA-bipy ligand changes the steepness of the spin transition and/or the spin transition temperature $T_{1/2}$ whereas the 4-PABipy ligand modifies a one-step to a two-step transition. In contrast to **1a** where the two-step transition is centered around the $T_{1/2}$ value of the parent system **1**, the SCO curve of **2a** is shifted to higher temperatures with respect to **2**.

What is the reason for the high-temperature shift of $T_{1/2}$ of **2a** and **2b** as compared to **2**? Intramolecular electronic effects cannot explain this result as the investigation of **1a**, **1b** and **1c** showed that the 4- and 5-PABipy ligands exert a weaker ligand field than unsubstituted 2,2'-bipyridine. It has been shown that crystal packing of $[\text{Fe}(\alpha\text{-diimine})_2(\text{NCS})_2]$ complexes is determined by two kinds of intermolecular interactions: π - π interactions of the diimine ligands and "donor-acceptor" interactions between the sulfur atom of the isothiocyanate groups and two carbon atoms of a diimine ligand.^[41] In complexes **2a** and **2b** the electron density in the bipy coligands is reduced through introduction of phenylazo substituents, which in turn could entail a bigger charge donation from the thiocyanate groups and thus increase the strength of the intermolecular donor-acceptor

interactions. This effect would act to stabilize the low-spin state in **2a** and **2b** in comparison to **2**, because the volume increase during the spin transition would become more unfavorable.

In analogy to complexes **1a** and **1b**, LIESST experiments were performed in a SQUID magnetometer equipped with an irradiation unit. In contrast to the former systems, however, the light-induced high-spin state was not stable in the timescale of the experiment for **2a** and **2b** after switching off the light source. These results indicate a shorter lifetime of the metastable high-spin state than in **1a-1c**, in agreement with the inverse energy-gap law.^[16,17]

b) UV/Vis and Resonance-Raman Spectroscopy

In order to obtain further insight into the temperature and light-induced SCO behavior of **2a** and **2b** UV/Vis spectroscopy was performed on KBr pellets between 4 and 297 K (Figure 9). In the UV/Vis spectrum of complex **2a** at room temperature two major absorption features are observed (Figure 9, left, red). The more intense absorption band at 333 nm can be ascribed to the $\pi \rightarrow \pi^*$ transition of the 4-PABipy ligand.

The Fe \rightarrow 4-PABipy-MLCT transition appears around 700 nm which, compared to the parent complex **2**, corresponds to a bathochromic shift of about ca. 100 nm.^[34] The small intensity increase of the MLCT band upon cooling to 4 K indicates that **2a** mostly exists in the low-spin state at 300 K (Figure 9, left, blue), in agreement with the susceptibility data. This may also be the reason why no d \rightarrow d transition absorption band is detected around 890 nm like in $[\text{Fe}(\text{bipy})_2(\text{NCS})_2]$ at room temperature.^[34] After irradiation of the sample at 4 K with 519 nm the MLCT absorption band decreases by about 10 %, indicating the LIESST effect (Figure 9, left, green). Fast relaxation might be the reason for the small decrease of intensity, which is in accordance with the SQUID-measurements.

The Fe \rightarrow 5-PABipy MLCT transition of complex **2b** is also shifted to lower energies compared to the parent spin crossover complex.^[34] The intensity of the corresponding absorption band is smaller than for the Fe \rightarrow 4-PABipy transition in **2a** (Figure 9, right, red), in analogy to complexes **1a** and **1b**. Moreover, the high-spin fraction of **2b** is 50 % at 300 K. Therefore, only a relatively minor intensity change occurs upon cooling down

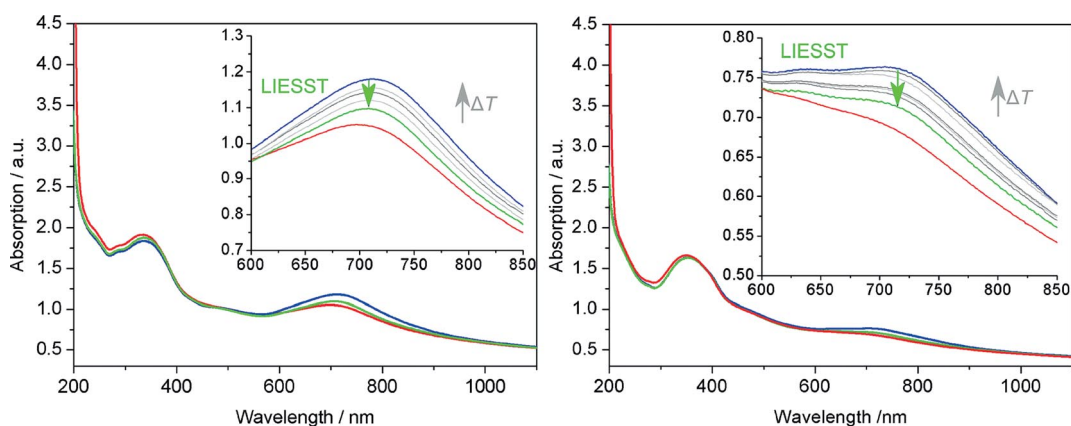


Figure 9. UV/Vis spectra of complex **2a** (left) and **2b** (right) in KBr. Red: room temperature spectrum, green: Irradiation with 519 nm at 4 K for 2 min, Blue: 4 K spectrum. Inset: detailed view on the MLCT transition.

from 300 to 2 K (Figure 9, right, blue). Irradiation of the sample with 519 nm at 4 K leads to a small intensity decrease of the MLCT absorption band (Figure 9, right, green). This indicates a partial population of the metastable high-spin state.

Thus, UV/Vis spectroscopy at cryogenic temperatures on complexes **2a** and **2b** in principle indicates LIESST behavior for both complexes, although for both systems the effect is small. So, we decided to study the spin-switching properties of these [Fe(PABipy)₂(NCS)₂] complexes by temperature-dependent resonance Raman spectroscopy, anticipating that permanent irradiation of the sample by the exciting laser might enable monitoring the metastable high-spin state also in the presence of fast relaxation, as already exemplified for thin films of a series of [Fe(bpz)₂(L)] complexes.^[14,42] In particular the C=N stretching frequencies of the isothiocyanate coligands should serve as a sensitive probe to monitor the spin state of the iron(II) metal center.^[34,69–73]

For the resonance Raman experiments KBr pellets of complexes **2a** and **2b** were prepared, and overview spectra were recorded at room temperature to determine the most suitable excitation wavelength. Afterwards, the samples were cooled down to 30 K. Resonance-Raman spectra were collected at low temperature and during warm-up of the sample in a frequency range from 2425 to 1725 cm⁻¹ (Figures 10 and 11).

In case of complex **2a** we used 514 nm as excitation wavelength λ_{exc} . In the temperature range from 40 K to 300 K thermal spin crossover as well as LIESST-behavior could be observed (Figure 10, left). At 40 K (dark) the dominant stretching vibration is located at ca. 2070 cm⁻¹, which corresponds to the light-induced metastable high-spin state. Obviously, not all molecules are excited to the high-spin state, because the low-spin vibrational mode is present at 2100 cm⁻¹, although with low intensity.^[34,69–73] Above 40 K the high-spin vibration band disappears and the low-spin band becomes dominant, due to relaxation which becomes faster at higher temperatures (Figure 10, right). Between 110 and 250 K the sample exists in the low-spin state. At 260 K the intensity of the low-spin vibrational mode decreases and the high-spin stretch at 2070 cm⁻¹ appears again. At 300 K both spin states are present with comparable intensities.

Resonance-Raman data recorded for **2b** in the temperature range from 42 to 284 K and with an excitation wavelength of 488 nm show the thermal spin crossover and LIESST effect as well (Figure 11, left). At 42 K a very intense high-spin C=N stretch is observed at 2066 cm⁻¹. In the temperature range from 42–70 K the metastable high-spin state prevails; a small population of the low-spin state is indicated by a vibration at 2119 cm⁻¹. From 117 K to 155 K the intensity of the low-spin

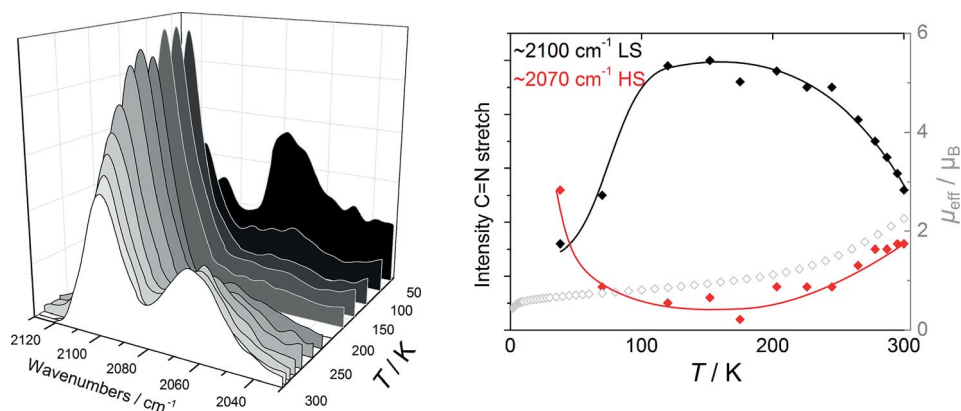


Figure 10. Resonance-Raman spectra of complex **2a** (left, $\lambda_{\text{exc}} = 514$ nm) and intensity of the C=N stretching vibration of the low-spin (black) and the high-spin state (red) as a function of temperature (right). Grey circles represent the susceptibility data out of Figure 8 in the temperature from 5–300 K (right). The solid lines serve as a guide to the eye.

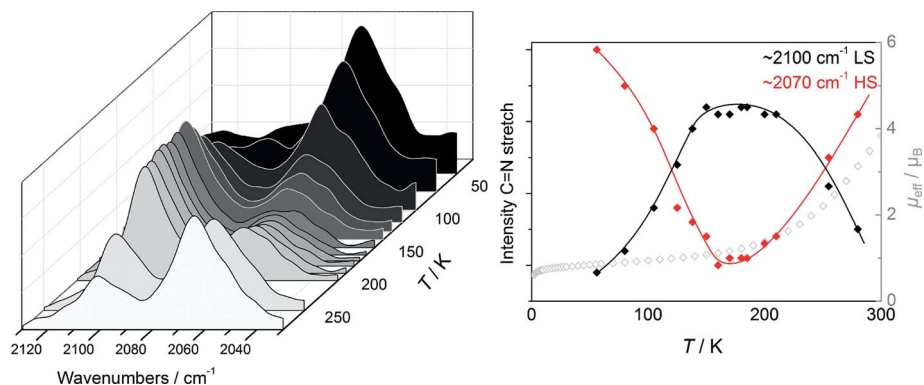


Figure 11. Resonance-Raman spectra of complex **2b** (left, $\lambda_{\text{exc}} = 488$ nm) and intensity of the C=N stretching vibration of the low-spin (black) and the high-spin state (red; right). Grey circles represent the susceptibility data of **2b** in the temperature from 5–300 K (right). The solid lines serve as a guide to the eye.

vibration increases such that it becomes more intense than the high-spin vibration. Nevertheless, there is a small high-spin fraction present. Till 194 K the intensity ratio of both vibrational modes remains constant. From 205 K the intensity of the high-spin stretch at 2066 cm^{-1} increases continuously (Figure 11, right). At room temperature, the high-spin intensity is higher than the low-spin intensity, but the spin transition is not complete yet, in agreement with the magnetic susceptibility data.

Conclusions

Attachment of phenylazo units in 4- and 5-position of 2,2'-bipyridine leads to characteristic changes in the SCO properties of classic Fe^{II} complexes with one or two bipy coligands: (i) global shifts of the SCO curve to higher or to lower temperatures with or without hysteresis, (ii) appearance of two-step transitions which are absent in the parent systems, and (iii) almost complete suppression of thermal SCO. These findings can be attributed to a combination of intra- and intermolecular interactions. An important intramolecular factor is the ligand field strength which in 4-PAbipy is almost equal to and in 5-PAbipy is reduced with respect to the unsubstituted bipy ligand. Furthermore, the different PAbipy ligands influence the cooperativity in the bulk material through short- and long-range interactions. Whereas these interactions generally render spin transitions in solids steeper than in solution, they can also act to suppress spin transitions in crystalline lattices by blocking relative motions of complex molecules. Such an effect has been exemplified for **1c**, where also temperature-induced excited spin state trapping (TIESST) could be observed. A further possible influence of intermolecular interactions could be evidenced for **2a** and **2b** where the shift of $T_{1/2}$ towards higher temperature with respect to the parent system **2** is attributed to an increased strength of intermolecular donor-acceptor interactions.

For all investigated systems, evidence for the LIESST effect was observed at cryogenic temperatures. In agreement with the inverse energy-gap law, the lifetimes of the metastable high-spin states were found to be much larger in the bpz complexes **1a–1c** than in their $[\text{Fe}(\text{PAbipy})_2(\text{NCS})_2]$ counterparts **2a** and **2b**. Nevertheless, a dynamic population of the metastable high-spin state by continuous laser excitation could also be detected for the latter systems in resonance Raman measurements.

Experimental Section

General: The Stille-type coupling reactions and the complex syntheses were performed under an inert gas atmosphere using Schlenk techniques. The solvents were dried and freshly distilled under inert gas. The syntheses of the stannylated pyridines and the further ligand syntheses were prepared analogous to literature-known procedures.^[46–49,74] The syntheses of the $[\text{Fe}(\text{bpz})_2(\text{L})]$ complexes were prepared using literature procedure as well.^[26] All chemicals were reagent grade from Aldrich or abcr. Elemental analyses were performed using a Euro Vector CHNS-O-elemental analyzer (Euro EA 3000). Samples were burned in sealed tin containers by a stream of oxygen. ^1H - and ^{13}C -NMR spectra were recorded with

Bruker Avance 400 and a Bruker Avance 200 at room temperature and are referenced to the solvent or TMS.

Magnetic susceptibility data were obtained from powdered samples using a Quantum-Design MPMS-5 SQUID magnetometer equipped with a 5 Tesla magnet in the range from 400 to 2 K. For the LIESST effect studies the fiber optic sample holder (FOSH, Quantum Design) with a 200 W Hg(Xe) arc lamp, a filter wheel (filter 510 nm, fwhm: 80 nm), shutter and a multicore fibre (all LOT Oriel) was used. The temperature was scanned with 2 K/min at an applied field of 5000 Oe. As the exact amount of sample in the FOSH sample cell is difficult to measure and to estimate the correction for sample holder and diamagnetism of the sample, the sample mass is calculated from scaling the data to the experimental data from the normal measurements for the temperature range 300 to 280 K. The magnetic measurements without irradiation were performed with an automated low-temperature physical property measurement system (PPMS, Quantum Design). Diamagnetic corrections were applied with the use of the tabulated Pascal's constants. Mössbauer spectra were recorded on a WISSEL Mössbauer setup equipped with an Oxford cryostat. The UV/Vis experiments were performed on a Cary5000 spectrometer in transmission geometry. For temperature dependence a CryoVac Kryostat with helium cooling was used. For illumination experiments $3\times$ LED Luxeon Typ LXML-PM01-0080 (519 nm) was used from Sahlmann Photochemical Solutions. Before the samples were cooled down to 4 K a room temperature spectrum was recorded. After measuring of the 4 K spectrum the sample was irradiated with 519 nm for 2 min leading to the metastable situation. After the irradiation and recollection of the thermal relaxation spectra the samples were warmed up to room temperature and another 300 K UV/Vis-spectra was recorded to assure the intactness of the samples. For Raman spectroscopic measurements a Dilor XY-Raman spectrometer (Horiba) was used with an Ar^+/Kr^+ mixed gas laser (SpectraPhysics GmbH) operating at 514 nm and 488 nm.

2-Bromo-(4-phenylazo)pyridine: 4-Amino-5-bromopyridine (2.0 g, 11.6 mmol) was dissolved in 75 mL of pyridine, 33.3 mL (92.8 mmol) 25 % TMAH solution was added, and heated to 80 °C. Nitrosobenzene 1.24 g (11.6 mmol) was solved in 40 mL of pyridine, added dropwise and heated at 80 °C for 4 h. After cooling the solution was extracted 3 times with toluene. The combined organic phases were dried with MgSO_4 and the solvent removed in vacuo. The residue was chromatographed (column, SiO_2), by eluting with cyclohexane/EtOAc: 1/3/1 % TEA, yield 2.18 g (6.39 mmol, 61 %). $\text{C}_{11}\text{H}_8\text{BrN}_3$ (262.11): calcd. C 50.4, H 3.1, N 16.0; found C 50.4, H 3.1, N 15.5. ^1H NMR (200 MHz, CDCl_3 , TMS): δ = 8.55 (dd, 3J = 5.2, 5J = 0.6 Hz, 1 H), 8.02–7.96 (m, 2 H), 7.89 (dd, 4J = 1.7, 5J = 0.6 Hz, 1 H), 7.70 (dd, 1 H, 3J = 5.2, 4J = 1.7 Hz, 1 H), 7.55 (m, 3 H) ppm. ^{13}C NMR (101 MHz, CDCl_3 , TMS): δ = 158.9 (C_q), 152.3 (C_q), 151.5 (C_i), 143.3 (C_q), 133.1 (C_i), 129.5 (C_i), 123.8 (C_i), 120.5 (C_i), 116.6 (C_i) ppm.

2-Bromo-(5-phenylazo)pyridine: To a solution of 1.50 mg (8.67 mmol) 5-amino-2-bromopyridine and 947 mg (8.85 mmol) nitrosobenzene in 60 mL of pyridine 354 mg (8.85 mmol) sodium hydroxide in 2 mL of water was added under continuous stirring. After 24 h 60 mL of water was added and the solution was extracted 2 times with 150 mL of toluene. The combined organic phases were dried with MgSO_4 and the solvent removed in vacuo. The residue was chromatographed (column, SiO_2), by eluting with cyclohexane/EtOAc: 1/3/2 % TEA, yield 1.68 g (6.42 mmol, 74 %). $\text{C}_{11}\text{H}_8\text{BrN}_3$ (262.11): calcd. C 50.4, H 3.1, N 16.0; found C 50.7, H 3.2, N 15.6. ^1H NMR (400 MHz, CDCl_3): δ = 8.96 (dd, 4J = 2.6, 5J = 0.6 Hz, 1 H), 8.01 (dd, 3J = 8.5, 4J = 2.6 Hz, 1 H), 7.97–7.90 (m, 2 H), 7.62 (dd, 3J = 8.5, 5J = 0.6 Hz, 1 H, 1 H), 7.57–7.51 (m, 3 H) ppm. ^{13}C NMR (75 MHz,

CDCl_3 : $\delta = 152.4$ (C_q), 148.2 (C_t), 147.2 (C_q), 144.1 (C_q), 132.2 (C_t), 129.4 (C_t), 129.1 (C_t), 128.8 (C_t), 123.3 (C_t) ppm.

(4-Phenylazo)-2,2'-bipyridine (4-PAbipy): Through a mixture of 1.80 g (6.90 mmol) 2-bromo-(4-phenylazo)pyridine and 1.1 mL (6.20 mmol) (2-trimethylstannyl)pyridine in 30 mL of *m*-xylene was degassed by an N_2 -stream for 1 h. After the addition of 80 mg (1 mol-%) $[\text{Pd}(\text{PPh}_3)_4]$ the solution was heated to 140 °C for 15 h. After cooling down to room temperature the mixture was added to 40 mL of 2 N sodium hydroxide solution and the phases were separated. The aqueous phase was extracted 2 times with 150 mL of toluene and the organic phases were dried with MgSO_4 and the solvent was removed in vacuo. The residue was chromatographed (column, SiO_2), by eluting with cyclohexane/EtOAc: 1/3/2 % TEA, yield 1.43 g (5.50 mmol, 80 %). $\text{C}_{16}\text{H}_{12}\text{N}_4$ (260.30): calcd. C 73.8, H 4.7, N 21.5; found C 73.4, H 4.6, N 21.0. ^1H NMR (400 MHz, $[\text{D}_8]$ toluene): $\delta = 9.31$ (dd, $^4J = 1.9$, $^5J = 0.7$ Hz, 1 H), 8.65 (ddd, $^3J = 8.0$, $^4J = 1.2$, $^5J = 0.9$ Hz, 1 H), 8.61 (dd, $^3J = 5.1$, $^5J = 0.7$ Hz, 1 H), 8.51 (ddd, $^3J = 4.7$, $^4J = 1.8$, $^5J = 0.9$ Hz, 1 H), 7.88 (m, 2 H), 7.46 (dd, $^3J = 5.1$, $^4J = 1.9$ Hz, 1 H), 7.24 (ddd, $^3J = 8.0$, $^3J = 7.5$, $^4J = 1.8$ Hz, 1 H), 7.12 (m, 3 H), 6.73 (ddd, $^3J = 7.5$, $^3J = 4.7$, $^4J = 1.2$ Hz, 1 H) ppm. ^{13}C NMR (75 MHz, CDCl_3): $\delta = 158.6$ (C_q), 158.3 (C_q), 155.8 (C_q), 152.5 (C_q), 150.8 (C_t), 149.5 (C_t), 137.2 (C_t), 132.5 (C_t), 129.4 (C_t), 124.2 (C_t), 123.6 (C_t), 121.4 (C_t), 116.3 (C_t), 114.1 (C_t) ppm.

(5-Phenylazo)-2,2'-bipyridine (5-PAbipy): Through a mixture of 642 mg (2.65 mmol) 2-bromo-5-(phenylazo)pyridine and 0.45 mL (2.40 mmol) (2-trimethylstannyl)pyridine in 30 mL of *m*-xylene was degassed by an N_2 stream for 1 h. After the addition of 31 mg (1 mol-%) $[\text{Pd}(\text{PPh}_3)_4]$ the solution was heated to 120 °C for 20 h. After cooling down to room temperature the mixture was added to 40 mL of 2 N sodium hydroxide solution and the phases were separated. The aqueous phase was extracted 2 times with 70 mL of toluene and the organic phases were dried with MgSO_4 and the solvent was removed in vacuo. The residue was chromatographed (column, SiO_2), by eluting with cyclohexane/EtOAc: 1/3/2 % TEA, yield 468 mg (1.79 mmol, 68 %). $\text{C}_{16}\text{H}_{12}\text{N}_4$ (260.30): calcd. C 73.8, H 4.7, N 21.5; found C 74.1, H 4.7, N 21.7. ^1H NMR (400 MHz, $[\text{D}_8]$ toluene): $\delta = 9.36$ (dd, $^4J = 2.4$, $^5J = 0.7$ Hz, 1 H), 8.74 (dd, $^3J = 8.6$, $^5J = 0.7$ Hz, 1 H), 8.65 (ddd, $^3J = 8.0$, $^4J = 1.2$, $^5J = 0.9$ Hz, 1 H), 8.49 (ddd, $^3J = 4.7$, $^4J = 1.8$, $^5J = 0.9$ Hz, 1 H), 8.02 (dd, $^3J = 8.5$, $^4J = 2.4$ Hz, 1 H), 7.90 (m, 2 H, 8-H), 7.22 (ddd, $^3J = 8.0$, $^3J = 7.5$, $^4J = 1.8$ Hz, 1 H), 7.15 (m, 3 H), 6.72 (ddd, $^3J = 7.5$, $^3J = 4.7$, $^4J = 1.2$ Hz, 1 H) ppm. ^{13}C NMR (126 MHz, CDCl_3): $\delta = 158.0$ (C_q), 155.5 (C_q), 152.8 (C_q), 149.5 (C_t), 147.9 (C_q), 147.5 (C_t), 137.2 (C_t), 131.9 (C_t), 129.4 (C_t), 127.6 (C_t), 124.3 (C_t), 123.1 (C_t), 121.8 (C_t), 121.7 (C_t) ppm.

4'-tBu-(5-Phenylazo)-2,2'-bipyridine ($^t\text{Bu}5\text{-PAbipy}$): A solution of 800 mg (3.05 mmol) 2-bromo-5-(phenylazo)pyridine and 176 mg (153 μmol) $[\text{Pd}(\text{PPh}_3)_4]$ in 20 mL of toluene was stirred for 20 min. Afterwards 1.29 g (3.05 mmol) 2-(tributylstannyl)pyridine was added and the solution was heated for 12 h at 135 °C. After the reaction was cooled to room temperature the suspension was filtered through celite. 20 mL of satd. NaHCO_3 solution was added and the org. layer was separated. Then the aqueous phase were extracted with dichloromethane. After combining of the org. phases the solution was dried with MgSO_4 and the solvent was removed in vacuo. The residue was chromatographed (column, SiO_2), by eluting with cyclohexane/EtOAc: 10/1/2 % TEA, yield 614 mg (1.94 mmol, 64 %). $\text{C}_{20}\text{H}_{20}\text{N}_4$ (316.40): calcd. C 75.9, H 6.4, N 17.7; found C 76.2, H 6.6, N 17.6. ^1H NMR (400 MHz, $[\text{D}_8]$ toluene): $\delta = 9.41$ (dd, $^4J = 2.4$, $^5J = 0.7$ Hz, 1 H), 8.91 (dd, $^4J = 2.0$, $^5J = 0.7$ Hz, 1 H), 8.85 (dd, $^3J = 8.6$, $^5J = 0.7$ Hz, 1 H), 8.54 (dd, $^3J = 5.2$, $^5J = 0.7$ Hz, 1 H), 8.06 (dd, $^3J = 8.6$, $^4J = 2.4$ Hz, 1 H), 7.90 (m, 2 H), 7.15 (m, 3 H), 6.91 (dd, $^3J = 5.2$, $^4J = 2.0$ Hz), 1.14 (s, 9 H) ppm. ^{13}C NMR

(75 MHz, $[\text{D}_8]$ toluene): $\delta = 160.7$ (C_q), 158.9 (C_q), 155.8 (C_q), 153.2 (C_q), 149.7 (C_t), 148.1 (C_q), 147.7 (C_t), 131.6 (C_t), 129.2 (C_t), 127.4 (C_t), 123.5 (C_t), 121.9 (C_t), 121.4 (C_t), 118.9 (C_t), 34.8 (C_q), 30.5 (C_s) ppm.

$[\text{Fe}(\text{bpz})_2(4\text{-PAbipy})]$ (1a): To a solution of 150 mg (0.41 mmol) iron(II) perchlorate hexahydrate in 5 mL of methanol 153 mg (0.82 mmol) potassium dihydro(bispyrazolyl)borate, dissolved in 5 mL of methanol, was added. After 15 min the precipitated KClO_4 was removed by filtration and washed with 5 mL of methanol. A solution of 107 mg (0.41 mmol) 4-(phenylazo)-2,2'-bipyridine in 10 mL of methanol was added dropwise. A greenish precipitate was yielded after filtration, washing with methanol and dried in vacuo, yield 141 mg (230 μmol , 56 %). $\text{C}_{28}\text{H}_{28}\text{B}_2\text{FeN}_{12}$ (610.08): calcd. C 55.1, H 4.6, N 27.6; found C 54.7, H 4.9, N 27.2.

$[\text{Fe}(\text{bpz})_2(5\text{-PAbipy})]$ (1b): To a solution of 726 mg (2 mmol) iron(II) perchlorate hexahydrate in 10 mL of methanol 744 mg (4.00 mmol) potassium dihydro(bispyrazolyl)borate, dissolved in 10 mL of methanol, was added. After 15 min the precipitated KClO_4 was removed by filtration and washed with 5 mL of methanol. A solution of 521 mg (2.00 mmol) 5-(Phenylazo)-2,2'-bipyridine in 10 mL of methanol was added dropwise. A greenish precipitate was yielded after filtration, washing with methanol and dried in vacuo, yield 673 mg (1.10 mmol, 55 %). $\text{C}_{28}\text{H}_{28}\text{B}_2\text{FeN}_{12}$ (610.08): calcd. C 55.1, H 4.6, N 27.6; found C 55.0, H 4.9, N 27.3.

$[\text{Fe}(\text{bpz})_2(^t\text{Bu}5\text{-PAbipy})]$ (1c): To a solution of 150 mg (413 μmol) iron(II) perchlorate hexahydrate in 5 mL of methanol 154 mg (828 μmol) potassium dihydro(bispyrazolyl)borate, dissolved in 5 mL of methanol, was added. After 15 min the precipitated KClO_4 was removed by filtration and washed with 5 mL of methanol. A solution of 133 mg (420 μmol) 4'-tBu-5-(phenylazo)-2,2'-bipyridine in 20 mL of methanol was added dropwise. A greenish precipitate was yielded after filtration, washing with methanol and dried in vacuo, yield 92.0 mg (138 μmol , 33 %). $\text{C}_{32}\text{H}_{36}\text{B}_2\text{FeN}_{12}$ (666.18): calcd. C 57.7, H 5.5, N 25.2; found C 58.2, H 5.6, N 25.2.

$[\text{Fe}(4\text{-PAbipy})_2(\text{NCS})_2]$ (2a): In a 100 mL Schlenk flask 100 mg (0.28 mmol) iron(II) trifluoromethanesulfonate and 55.0 mg (0.57 mmol) potassium thiocyanate were mixed in 5 mL of CH_3CN . Afterwards 221 mg (0.85 mmol) 5-(phenylazo)-2,2'-bipyridine, dissolved in 20 mL of warm CH_3CN , were added and the mixture was heated to 80 °C for 3 h. After cooling down a blue solid was filtered off and dried in vacuo, yield 170 mg (0.25 mmol, 88 %). $\text{C}_{34}\text{H}_{24}\text{FeN}_{10}\text{S}_2$ (692.60): calcd. C 59.0, H 3.5, N 20.2, S 9.3; found C 58.7, H 3.3, N 19.8, S 9.5.

$[\text{Fe}(5\text{-PAbipy})_2(\text{NCS})_2]$ (2b): In a 100 mL Schlenk flask 100 mg (0.28 mmol) iron(II) trifluoromethanesulfonate and 55.0 mg (0.57 mmol) potassium thiocyanate were mixed in 5 mL of CH_3CN . Afterwards 221 mg (0.85 mmol) 5-(phenylazo)-2,2'-bipyridine, dissolved in 20 mL of warm CH_3CN , were added and the mixture was heated to 80 °C for 3 h. After cooling down a green solid was filtered off and dried in vacuo, yield 158 mg (0.22 mmol, 81 %). $\text{C}_{34}\text{H}_{24}\text{FeN}_{10}\text{S}_2$ (692.60): calcd. C 59.0, H 3.5, N 20.2, S 9.3; found C 58.6, H 3.4, N 20.4, S 9.5.

Acknowledgments

F. T. thanks Deutsche Forschungsgemeinschaft (DFG) for funding this research (SFB 677). The authors thank Dr. Luca Carella and Prof. E. Rentschler (Johannes Gutenberg University Mainz) for the SQUID-measurements on the complex $[\text{Fe}(\text{bpz})_2(\text{bipy})]$. The authors thank Maren Rasmussen and Henning Lühmann for the TIESST experiments. S. O. S. also thanks Tammy Jacob-

sen-Bialas for synthetic work and Stephanie Pehlke for recording resonance Raman measurements.

Keywords: Iron · Spin crossover · Magnetic properties · Moessbauer spectroscopy · Resonance Raman spectroscopy · LIESST

- [1] L. Cambi, L. Szegő, *Ber. Dtsch. Chem. Ges.* **1931**, *64*, 2591.
- [2] P. Gütllich, A. Hauser, H. Spiering, *Angew. Chem. Int. Ed. Engl.* **1994**, *33*, 202024, 2024–2054–2141; *Angew. Chem.* **1994**, *106*, 2109; P. Gütllich, H. A. Goodwin, *Spin Crossover in Transition Metal Compounds I–III*, *Top. Curr. Chem.*, Springer, Berlin, **2004**, vol. 233–235; P. Gütllich, H. A. Goodwin, *Top. Curr. Chem.* **2004**, 233–235.
- [3] O. Kahn, J. Kröber, C. Jay, *Adv. Mater.* **1992**, *4*, 718–728.
- [4] S. Sanvito, *Chem. Soc. Rev.* **2011**, *40*, 3336–3355.
- [5] J. Letard, P. Guinneau, L. Goux-Capes, *Top. Curr. Chem.* **2004**, *235*, 221–249.
- [6] A. Bousseksou, G. Molnar, L. Salmon, W. Nicolazzi, *Chem. Soc. Rev.* **2011**, *40*, 3313–3335.
- [7] M. C. Munoz, J. A. Real, *Coord. Chem. Rev.* **2011**, *255*, 2068–2093.
- [8] M. A. Halcrow, *Spin-Crossover Materials – Properties and Applications*, Wiley-VCH, Weinheim, Germany, 1st ed., **2013**.
- [9] O. Kahn, C. J. Martinez, *Science* **1998**, *279*, 44–48.
- [10] S. Decurtins, P. Gütllich, C. P. Köhler, H. Spiering, A. Hauser, *Chem. Phys. Lett.* **1984**, *105*, 1–4.
- [11] M.-L. Boillot, J. Zarembowitch, A. Sour, *Top. Curr. Chem.* **2004**, *234*, 261–276.
- [12] S. Thies, H. Sell, C. Schütt, C. Bornholdt, C. Näther, F. Tuzcek, R. Herges, *J. Am. Chem. Soc.* **2011**, *133*, 16243–16250; S. Thies, C. Bornholdt, F. Köhler, F. Soennichsen, C. Näther, F. Tuzcek, R. Herges, *Chem. Eur. J.* **2010**, *16*, 10074–10083.
- [13] S. Venkataramani, U. Jana, M. Dommaschk, F. D. Sönnichsen, F. Tuzcek, R. Herges, *Science* **2011**, *331*, 445–448.
- [14] E. Ludwig, H. Naggert, M. Källäne, S. Rohlf, S. Kröger, A. Bannwarth, A. Quer, K. Rossnagel, L. Kipp, F. Tuzcek, *Angew. Chem. Int. Ed.* **2014**, *53*, 11, 3019–3023; *Angew. Chem.* **2014**, *126*, 3063–3067.
- [15] A. Witt, F. W. Heinemann, M. M. Khusniyarov, *Chem. Sci.* **2015**, *6*, 4599–4609.
- [16] A. Hauser, *Coord. Chem. Rev.* **1991**, *111*, 275–290.
- [17] A. Hauser, C. Enachescu, M. Lawson Daku, A. Vargas, N. Amstutz, *Coord. Chem. Rev.* **2006**, *250*, 1642–1652.
- [18] Y. Hasegawa, S. Kume, H. Nishihara, *Dalton Trans.* **2009**, 280–284.
- [19] M. Milek, F. W. Heinemann, M. M. Khusniyarov, *Inorg. Chem.* **2013**, *52*, 11585–11592.
- [20] N. Matsumoto, S. Ohta, C. Yoshimura, A. Ohyoshi, S. Kohata, H. Okawa, Y. Maeda, *J. Chem. Soc., Dalton Trans.* **1985**, 2575–2584.
- [21] A. Sour, M.-L. Boillot, E. Riviere, P. Lesot, *Eur. J. Inorg. Chem.* **1999**, 2117–2119.
- [22] S. Hirose, S. Hayami, Y. Maeda, *Bull. Chem. Soc. Jpn.* **2000**, *73*, 2059–2066.
- [23] C. Krüger, P. Augustin, I. Nemeč, Z. Travnicek, H. Oshio, R. Boca, F. Renz, *Eur. J. Inorg. Chem.* **2013**, 902–915.
- [24] C. Krüger, P. Augustin, L. Dhan, J. Pavlik, J. Moncol, I. Nemeč, R. Boca, F. Renz, *Polyhedron* **2015**, *87*, 194–201.
- [25] A. Bannwarth, S. O. Schmidt, G. Peters, F. D. Sönnichsen, W. Thimm, R. Herges, F. Tuzcek, *Eur. J. Inorg. Chem.* **2012**, 2776–2783.
- [26] J. A. Real, M. C. Munoz, J. Faus, X. Solans, *Inorg. Chem.* **1997**, *36*, 3008–3013.
- [27] H. Naggert, A. Bannwarth, S. Chemnitz, T. von Hofe, E. Quandt, F. Tuzcek, *Dalton Trans.* **2011**, *40*, 6364–6366.
- [28] T. G. Gopakumar, F. Matino, H. Naggert, A. Bannwarth, F. Tuzcek, R. Berndt, *Angew. Chem. Int. Ed.* **2012**, *51*, 25, 6262–6266; *Angew. Chem.* **2012**, *124*, 6367–6371.
- [29] T. G. Gopakumar, M. Bernien, H. Naggert, F. Matino, C. F. Hermanns, A. Bannwarth, S. Mühlenberend, A. Krüger, D. Krüger, F. Nickel, W. Walter, R. Berndt, W. Kuch, F. Tuzcek, *Chem. Eur. J.* **2013**, *19*, 15702–15709.
- [30] B. Rösner, M. Milek, A. Witt, B. Gobaut, P. Torelli, R. H. Fink, M. M. Khusniyarov, *Angew. Chem. Int. Ed.* **2015**, *54*, 44, 12976–12980; *Angew. Chem.* **2015**, *127*, 13168–13172.
- [31] R. Kulmaczewski, H. J. Shepherd, O. Cespedes, M. A. Halcrow, *Inorg. Chem.* **2014**, *53*, 9809–9817.
- [32] M. Bernien, H. Naggert, L. M. Arruda, L. Kippen, F. Nickel, J. Miguel, C. F. Hermanns, A. Krüger, D. Krüger, E. Schierle, E. Weschke, F. Tuzcek, W. Kuch, *ACS Nano* **2015**, *9*, 8960–8966.
- [33] W. A. Baker Jr., H. M. Bobonich, *Inorg. Chem.* **1964**, *3*, 1184–1188.
- [34] E. König, K. Madeja, K. J. Watson, *J. Am. Chem. Soc.* **1968**, *90*, 1146–1153.
- [35] E. W. Müller, H. Spiering, P. Gütllich, *Chem. Phys. Lett.* **1982**, *93*, 567–571.
- [36] S. O. Schmidt, *unpublished results*.
- [37] M.-L. Boillot, S. Chantraine, J. Zarembowitch, J.-Y. Lallemand, J. Prunet, *New J. Chem.* **1999**, *23*, 179–183.
- [38] C. P. Köhler, R. Jakobi, E. Meissner, L. Wiehl, H. Spiering, P. Gütllich, *J. Phys. Chem. Solids* **1990**, *51*, 239–247.
- [39] A. Hauser, J. Jeftic, H. Romstedt, R. Hinek, H. Spiering, *Coord. Chem. Rev.* **1999**, *190–192*, 471–491.
- [40] H. Spiering, T. Kohlhaas, H. Romstedt, A. Hauser, C. Bruns-Yilmaz, J. Kusz, P. Gütllich, *Coord. Chem. Rev.* **1999**, *190–192*, 629–647.
- [41] J. A. Real, A. B. Gaspar, V. Niel, M. C. Munoz, *Coord. Chem. Rev.* **2003**, *236*, 121–141.
- [42] H. Naggert, J. Rudnik, L. Kippen, M. Bernien, F. Nickel, L. M. Arruda, W. Kuch, C. Näther, F. Tuzcek, *J. Mater. Chem. C* **2015**, *3*, 7870–7877.
- [43] P. Guionneau, M. Marchivie, G. Bravic, J.-F. Letard, D. Chasseau, *Top. Curr. Chem.* **2004**, *234*, 97–128.
- [44] J.-F. Letard, *J. Mater. Chem.* **2006**, *16*, 2550–2559.
- [45] A. Ozarowski, B. R. McGarvey, A. B. Sarkar, J. E. Drake, *Inorg. Chem.* **1988**, *27*, 628–635; B. Gallois, J. A. Real, C. Hauw, J. Zarembowitch, *Inorg. Chem.* **1990**, *29*, 1152–1158; M. Konno, M. Mikami-Kido, *Bull. Chem. Soc. Jpn.* **1991**, *64*, 339–345; J. A. Real, B. Gallois, T. Granier, F. Suez-Panama, J. Zarembowitch, *Inorg. Chem.* **1992**, *31*, 4972–4979; J. A. Real, M. C. Munoz, E. Andres, T. Granier, B. Gallois, *Inorg. Chem.* **1994**, *33*, 3587–3594; J.-F. Letard, S. Montant, P. Guionneau, P. Martin, A. Le Calves, E. Freysz, D. Chasseau, R. Lapouyade, O. Kahn, *Chem. Commun.* **1997**, 745–746; J.-F. Letard, P. Guionneau, E. Codjovi, O. Lavastre, G. Bravic, D. Chasseau, O. Kahn, *J. Am. Chem. Soc.* **1997**, *119*, 10861–10862; Z. J. Zhong, J. Q. Tao, Z. Yu, C. Y. Dun, Y. L. Liu, X. Z. You, *J. Chem. Soc., Dalton Trans.* **1998**, 327–328; N. Moliner, M. C. Munoz, S. Letard, J.-F. Letard, X. Solans, R. Burriel, M. Castro, O. Kahn, J. A. Real, *Inorg. Chim. Acta* **1999**, *291*, 279–288; J. Klingele, D. Kaase, M. Schmucker, Y. Lan, G. Chastanet, J.-F. Letard, *Inorg. Chem.* **2013**, *52*, 6000–6010.
- [46] C. Brotschi, G. Mathis, C. J. Leumann, *Chem. Eur. J.* **2005**, *11*, 1911–1923.
- [47] S. H. Wadman, Y. M. van Leeuwen, R. W. A. Havenith, G. P. M. van Klink, G. van Koten, *Organometallics* **2010**, *29*, 5635–5645.
- [48] B. W. Michel, L. D. Steffens, M. S. Sigma, *J. Am. Chem. Soc.* **2011**, *133*, 8317–8325.
- [49] E. V. Brown, G. R. Granneman, *J. Am. Chem. Soc.* **1975**, *97*, 621–627.
- [50] Y. Uchida, R. Kajita, Y. Kawasaki, S. Oae, *Phosphorus Sulfur Silicon Relat. Elem.* **1994**, *93–94*, 405–409.
- [51] O. S. Wenger, L. M. Henling, M. W. Day, J. R. Winkler, H. B. Gray, *Polyhedron* **2004**, *23*, 2955–2958.
- [52] A. Amar, P. Savel, H. Akdas-Kilig, C. Katan, H. Meghezzi, A. Boueckkine, J.-P. Malval, J.-L. Fillaut, *Chem. Eur. J.* **2015**, *21*, 8262–8270.
- [53] G. Ritter, E. König, W. Irlar, H. A. Goodwin, *Inorg. Chem.* **1978**, *17*, 224–228.
- [54] H. A. Goodwin, K. H. Sugiyarto, *Chem. Phys. Lett.* **1987**, *139*, 470–474.
- [55] T. Buchen, P. Gütllich, H. A. Goodwin, *Inorg. Chem.* **1994**, *33*, 4573–4576.
- [56] T. Buchen, P. Gütllich, K. H. Sugiyarto, H. A. Goodwin, *Chem. Eur. J.* **1996**, *2*, 1134–1138.
- [57] N. Moliner, A. B. Gaspar, M. Carmen Munoz, V. Niel, J. Cano, J. A. Real, *Inorg. Chem.* **2001**, *40*, 3986–3991.
- [58] K. D. Murnaghan, C. Carbonera, L. Toupet, M. Griffin, M. M. Dirtu, C. Desplanches, Y. Garcia, E. Collet, J.-F. Letard, G. G. Morgan, *Chem. Eur. J.* **2014**, *20*, 5613–5618.
- [59] J.-F. Letard, R. Labardel, J. A. K. Howard, A. E. Goeda, D. Chasseau, O. Kahn, *Inorg. Chem.* **1998**, *37*, 4432–4441.
- [60] P. Gütllich, R. Link, A. Trautwein, *Mössbauer Spectroscopy and Transition Metal Chemistry*, Springer, Berlin, Heidelberg, New York, **1978**.
- [61] P. Adler, H. Spiering, P. Gütllich, *Inorg. Chem.* **1987**, *26*, 3840–3845.
- [62] P. Adler, H. Spiering, P. Gütllich, *Hyperfine Interact.* **1988**, *42*, 1033–1038.
- [63] P. Adler, A. Hauser, A. Vef, H. Spiering, P. Gütllich, *Hyperfine Interact.* **1989**, *47*, 343–356.

- [64] P. Adler, P. Poganiuch, H. Spiering, *Hyperfine Interact.* **1989**, *52*, 47–63.
- [65] F. Grandjean, G. J. Long, B. B. Hutchinson, L. Ohlhausen, P. Neill, J. D. Holcomb, *Inorg. Chem.* **1989**, *28*, 4406–4414.
- [66] L. H. Gade, *Koordinationschemie*, Wiley-VCH, Weinheim, Germany, 1st ed., **1998**.
- [67] V. Ksenofontov, G. Levchenko, H. Spiering, P. Gütllich, J.-F. Letard, Y. Bouhedja, O. Kahn, *Chem. Phys. Lett.* **1998**, *294*, 545–553.
- [68] P. Guionneau, J.-F. Letard, D. S. Yufit, D. Chasseau, G. Bravic, A. E. Goeta, J. A. K. Howard, O. Kahn, *J. Mater. Chem.* **1999**, *9*, 985–994.
- [69] W. A. Baker Jr., G. J. Long, *Chem. Commun.* **1965**, 368–369.
- [70] R. H. Herber, *Inorg. Chem.* **1987**, *26*, 173–178.
- [71] E. König, K. Madeja, *Spectrochim. Acta Part A* **1967**, *23*, 45–54.
- [72] M. Sorai, S. Seki, *J. Phys. Chem. Solids* **1974**, *35*, 555–570.
- [73] A. Bousseksou, J. J. McGarvey, F. Varret, J. A. Real, J.-P. Tuchagues, A. C. Dennis, M. L. Boillot, *Chem. Phys. Lett.* **2000**, *318*, 409–416.
- [74] S. Trofimenko, *J. Am. Chem. Soc.* **1967**, *89*, 3170–3177.

Received: October 30, 2015

Published Online: December 23, 2015